Apr 98

Progress Report for:

CONTRACTS N00014-96-1-0586 & N00014-97-1-0966

MOVING TARGET DETECTION AND MOTION ESTIMATION IN FOLIAGE USING ALONG TRACK MONOPULSE SYNTHETIC APERTURE RADAR IMAGING

AND

SIGNAL SUBSPACE PROCESSING OF UNCALIBRATED MTD-SARS

Submitted to:

Office of Naval Research
Program Officer William J. Miceli, ONR 3131
Ballston Centre Tower One
800 North Quincy Street
Arlington, VA 22217-5660

Administrative Grants Officer
Office of Naval Research Regional Office Boston
495 Summer Street, Room 103
Boston, MA 02210-2109

Director, Naval Research Laboratory
Attn: Code 2627
4555 Overlook Drive
Washingon, DC 20375-5326

Defense Technical Information Center
8725 John J. Kingman Road
STE 0944
Ft. Belvoir, VA 22060-6218

Distribution Statement:

Approved for public release.

Project Director:

Mehrdad Soumekh
Department of Electrical & Computer Engineering
State University of New York at Buffalo
Amherst, New York 14260
Phone: (716) 645-2422, extension 2138
Fax: (716) 645-3656
Email: msoum@eng.buffalo.edu

Contents

Progress Report:

Moving Target Detection and Motion Estimation in Foliage Using Along Track Monopulse Synthetic Aperture Radar Imaging

AND

Signal Subspace Processing of Uncalibrated MTD-SARs

Mehrdad Soumekh
Department of Electrical & Computer Engineering
State University of New York at Buffalo
Amherst, New York 14260

1a. Overview

This document describes the progress on the work performed for "Moving Target Detection and Motion Estimation in Foliage Using Along Track Monopulse Synthetic Aperture Radar Imaging," under Contract N00014-96-1-0586, and "Signal Subspace processing of Uncalibrated MTD-SARs," under Contract N00014-97-1-0966 for the Office of Naval Research for the period ending on 9/30/98.

Our main goal at this stage of the investigation was to test the relative merits of the proposed signal subpace method with a realistic SAR/ISAR database. For this purpose, we utilized the ISAR data of an airborne commercial aircraft; the ISAR data were collected by the radar group at the Navy's SPAWAR System Center, San Diego. In the first stage of our study, we used the non-overlapping block-based implementation of the signal subspace algorithm for registering two ISAR images of the aircraft which were formed via two separate slow-time segments of the target flight path. We also used the overlapping block-based signal subspace processing to estimate the motion field of the ISAR images. The study with the realistic ISAR data revealed interesting properties of the ISAR signatures of the refelctors, cavities and surface structure for an airborne target.

1b. Publications

The work has produced the following articles which contain a note on the support from the Office of Naval Research under Contracts N00014-96-1-0586 and N00014-97-1-0966:

M. Soumekh, "Signal subspace fusion of uncalibrated sensors with application in SAR and diagnostic medicine," accepted for publication in *IEEE Transactions on Image Processing.*

M. Soumekh, *Synthetic Aperture Radar Signal Processing,* New York: Wiley, 1999 (in print).

M. Soumekh, "Bistatic Synthetic Aperture Radar Imaging Using Wide-Bandwidth

Continuous-Wave Sources," *Proceedings of SPIE's International Symposium on Optical Science, Engineering and Instrumentation*, San Diego, July 1998.

S. Chou, M. Pollock and M. Soumekh, "On Target Resolvability from Single Tone Fringe Patterns of Digitally-Spotlighted SAR Image," *Proceedings of SPIE's International Symposium on Optical Science, Engineering and Instrumentation*, San Diego, July 1998.

M. Soumekh, "Moving Target Detection and Automatic Target Recognition via Signal Subspace Fusion of Images," *Proceedings of SPIE's Annual International Symposium on Aerospace/Defense Sensing, Simulation, and Controls*, pp. 145-153, Orlando, April 1998.

M. Soumekh, "Signal Subspace Registration of 3D Images," *Proceedings of SPIE's Medical Imaging*, pp. 312-319, San Diego, February 1998.

2. Effect of Uncalibrated and Unstable Radars

This project began with the study of an along-track monopulse SAR system for moving target detection. The monopulse SAR Moving Tragte Indicator (MTI), which was developed in [S97a], is a reliable measure for moving target detection in the SAR scene provided that ***the two radars are fully calibrated***; that is, there is no relative gain and phase ambiguity in the data collected by the two radars. This idealistic scenario, however, is never encountered in practice. In a realistic monopulse SAR system, the two radars exhibit different amplitude patterns (phase as well as gain) which vary with the radar frequency and the radar position (that is, the slow-time domain) [S99].

Moreover, these amplitude patterns could vary from one pulse transmission to another due to heat and other uncontrollable natural factors which affect the internal circuitry of the two radars; this is referred to as instability of the radar amplitude pattern. These subtle changes of the amplitude patterns of the radars are difficult to be detected and tracked, and are unknown to the user.

Another source of calibration error for the monopulse MTI statistic is the ***narrow-beamwidth*** approximation which we used to develop it. One of the primary application areas of along-track monopulse SAR is in moving target detection in foliage with ***wide-beamwidth*** FOPEN UHF radars. In these applications, the use of the narrowband-beamwidth approximation introduces undesirable phase differences between the two along-track monopulse images of a stationary target.

In [S99], we show that all of the above three sources of calibration errors (that is, uncalibrated monopulse radars, radar instability, and narrow-beamwidth approximation) in along-track monopulse SAR can be lumped together; the outcome results in the following

relationship between the two monopulse images for the n-th stationary target:

$$f_{bn}(x - x_n, y - y_n) = f_{mn}(x - x_n, y - y_n) \ ** \ h_n(x, y),$$

where $h_n(x, y)$ is an ***unknown*** two-dimensional impulse function in the spatial (x, y) domain.

The above model, which states that the ***point spread function*** of the two monopulse radars are different, is intuitively obvious to most radar engineers; a similar problem has been known to exist in the classical monopulse radar signal processing [Leo], [Sher], [Sko]. The signal subspace processing is a deterministic method for dealing with the effects of the above-mentioned unknown impulse function; this is briefly described in the following section.

3. Signal Subspace Registration of Uncalibrated SAR Images

In this section, we examine the problem of fusing or registering information in uncalibrated sensors. The approach is based on manipulating a system model with ***unknown*** parameters, which relates the outputs of two uncalibrated sensors, to develop a procedure to ***blindly*** calibrate the two outputs. This system model is identical to the system model which we presented in Section 2 to relate the two uncalibrated monopulse SAR images of a stationary target. Thus, the method is also applicable in moving target detection with uncalibrated along-track monopulse SARs. We will show the application of this approach in automatic registration of ISAR images.

3.1 System Model

Consider a sensory system which acquires one-dimensional or multidimensional information (snapshots) of a stationary scene at various time points. Our objective is to detect relative change in any two of these snapshots due to the presence of a foreign object (for example, a moving target in SAR, nonlinear motion in video, or a tumor in a biological structure). For our discussion, we consider two-dimensional snapshots (images). Suppose the image recorded by one sensor is $f_1(x, y)$, also called the ***reference*** image. Then, the recorded image by the other sensor, called the ***test*** image, is modeled via the following:

$$\begin{aligned} f_2(x, y) &= f_1(x, y) \ ** \ h(x, y) + f_e(x, y) \\ &= \int_u \int_v h(u, v) \ f_1(x - u, y - v) \ du \ dv + f_e(x, y), \end{aligned}$$

where $**$ denotes the two-dimensional convolution in the spatial (x, y) domain.

In the above model, $f_e(x, y)$ is the change caused by a foreign object. and $h(x, y)$ is an impulse response which represents the relative shift and blurring in the two images due to slight motion and/or change in the Point Spread Function (PSF) of the two sensors; these

two signals, that is, $f_e(x,y)$ and $h(x,y)$, are unknown. To provide a general analysis, the signals in the above model are assumed to be complex. A block diagram representation of this model is shown in Figure 1.

The above model states that the output of the second sensor $f_2(x,y)$ is linearly related to the output of the first sensor $f_1(x,y)$ and its shifted versions. There might also be cases in which the sensors exhibit nonlinearity over time [S97o]. Also, in some applications, the second snapshot could be a linearly-transformed (shifted, rotated and scaled) version of $f_1(x,y)$. To present the basic concept behind registration of uncalibrated images via signal subspace processing, we begin with the model in Figure 1. However, this approach can be applied to the other above-mentioned models (nonlinear sensors, target rotation and scaling, etc.) [S97o]. These will be discussed in the analysis of registering SAR images for automatic target recognition.

3.2 Signal Subspace Processing

Let $\hat{f}_2(x_i,y_j)$ be the projection of $f_2(x_i,y_j)$ into the linear subspace which is defined by $f_1(x_i,y_j)$ and $N-1$, where $N = N_x N_y$, of its shifted versions; that is,

$$\Psi = [\ f_1(x_i - m\Delta_x, y_j - n\Delta_y);\ m = -n_x,\ldots,n_x,\ n = -n_y,\ldots,n_y\ ].$$

Thus, it is sufficient to identify the signal subspace Ψ, and then obtain the projection of $f_2(x_i,y_j)$ into this signal subspace to construct $\hat{f}_2(x_i,y_j)$.

Let

$$\psi_\ell(x_i,y_j), \qquad \ell = 1,2,\ldots,N,$$

be a set of orthogonal basis functions which spans the linear signal subspace of Ψ; that is,

$$\Psi = [\ \psi_\ell(x_i,y_j);\ \ell = 1,2,\ldots,N\ ],$$

where

$$< \psi_\ell\ ,\ \psi_j\ > = \sum_i \sum_j \psi_\ell(x_i,y_j)\ \psi_j^*(x_i,y_j) = \begin{cases} 1, & \text{for } \ell = j; \\ 0, & \text{otherwise.} \end{cases}$$

(In the above, ψ^* is the complex conjugate of ψ.) To generate this signal subspace, one can use a variety of techniques, such as Gram-Schmidt, modified Gram-Schmidt, Householder, Givens orthogonalization procedure, singular value decomposition, etc.

The size of the signal subspace, that is, N, depends on the user's a priori knowledge of the number of the nonzero coefficients in the discrete model of the impulse response $h(x,y)$, that is, the size of PSF based on the accuracy of the imaging system data acquisition. For instance, if the discrete $h(x,y)$ contains (N_x,N_y) non-zero pixels, then we should select

$N = N_x N_y$. (As we pointed out earlier, a similar assignment/model for $h(x,y)$ is used in the adaptive filtering methods [Har].)

In practice, the exact value of $N_x N_y$ is not known. In this case, an estimate should be used based on the maximum anticipated degree of shift and calibration errors between the two sensors. For instance, in the along-track monopulse SAR for moving target detection, the knowledge of the parameter variations in the electronic circuitry of the two monopulse radars over time could be used.

The projection of the $f_2(x_i, y_j)$ into the basis function $\psi_\ell(x_i, y_j)$, which is identified by the series coefficient $f_{2\ell}$ ($\ell = 1, 2, \ldots, N$), is found via the following:

$$f_{2\ell} =< \ f_2 \ , \ \psi_\ell \ >= \sum_i \sum_j \ f_2(x_i, y_j) \ \psi_\ell^*(x_i, y_j).$$

The projection of $f_2(x_i, y_j)$ into the signal subspace Ψ is achieved via the following:

$$\hat{f}_2(x_i, y_j) = \sum_{\ell=1}^{N} \ f_{2\ell} \ \psi_\ell(x_i, y_j).$$

Finally, the signal subspace difference image, that is, the statistic for detecting the foreign object, is constructed by

$$\hat{f}_d(x_i, y_j) = f_2(x_i, y_j) - \hat{f}_2(x_i, y_j).$$

3.3 Estimating Calibration Error Impulse Function

If one desires, the impulse response can be computed via the following procedure. Let $g_j(x_i, y_j)$, $k = 1, \ldots, N$, represent the ordered version of the signals

$$[\ f_1(x_i - m\Delta_x, y_j - n\Delta_y); \ m = -n_x, \ldots, n_x, \ n = -n_y, \ldots, n_y \ ],$$

in the manner in which the orthogonalization (for example, Gram-Schmidt) procedure is implemented; the manner in which these shifted versions of $f_1(x_i, y_j)$ are ordered does not significantly alter the outcome.

We define an N by N matrix $\mathbf{F}_1$ whose elements are the projection of $g_j(x_i, y_j)$'s into $\psi_\ell(x_i, y_j)$'s; that is,

$$f_{1j\ell} =< \ g_j \ , \ \psi_\ell \ >= \sum_i \sum_j \ g_j(x_i, y_j) \ \psi_\ell^*(x_i, y_j).$$

In the Gram-Schmidt procedure, $\mathbf{F}_1$ is a lower triangular matrix since $f_{1j\ell} = 0$ for $k < \ell$. We also define the 1 by N vector $\mathbf{F}_2$ which is made up of the coefficients $f_{2\ell}$, $\ell = 1, \ldots, N$. Then, it can be shown that the following 1 by N vector:

$$\mathbf{H} = \mathbf{F}_2 \ \mathbf{F}_1^{-1}$$

contains the estimated impulse response coefficients $\hat{h}_{mn}$. (The ordering is the same as the ordering of $g_j(x_i, y_j)$'s.)

3.4 Application in MTD Monopulse SAR

An along-track monopulse SAR imaging system utilizes two radars for its data collection. One radar is used as a transmitter as well as a monostatic receiver. The other radar is used only as a bistatic receiver. In [S97a], we developed a signal processing algorithm of the two monostatic and bistatic databases of the along-track monopulse SAR system to obtain two *coherently* identical SAR images of the stationary targets in the scene. While the stationary targets appear the same in the monostatic and bistatic SAR images, the same is not true for moving targets.

This fact is the basis for developing an MTI statistic, which we refer to as the difference image, for moving target detection. For a stationary n-th target, if we denote the monostatic SAR image by $f_{\mathrm{m}n}(x - x_n, y - y_n)$ and the bistatic image by $f_{\mathrm{b}n}(x, y)$, the difference image for moving target detection is defined via the following:

$$f_{\mathrm{d}n}(x - x_n, y - y_n) = f_{\mathrm{b}n}(x - x_n, y - y_n) - f_{\mathrm{m}n}(x - x_n, y - y_n).$$

In Section 2, we developed a model for the undesirable variations of the amplitude pattern of uncalibrated monopulse radars. Such a model indicates that the monopulse SAR images are related via

$$f_{\mathrm{b}n}(x - x_n, y - y_n) = f_{\mathrm{m}n}(x - x_n, y - y_n) \ ** \ h_n(x, y),$$

where $h_n(x, y)$ is a function of the calibration error of the two radars. This model is the same as the model in Figure 1 of the discussion of uncalibrated images in the previous section with

$$\begin{aligned} f_1(x, y) &= f_{\mathrm{m}n}(x - x_n, y - y_n) \\ f_2(x, y) &= f_{\mathrm{b}n}(x - x_n, y - y_n) \\ h_n(x, y) &= h(x, y), \end{aligned}$$

for a stationary n-th target, when there is no moving target (foreign object), that is, $f_e(x, y) = 0$.

Thus, the signal subspace method described in Section 3.1-3.3 can also be applied in the MTD monopulse SAR problem with uncalibrated radars. Note that the calibration error function for the MTD monopulse SAR and, thus, the impulse function $h_n(x, y)$ varies with the coordinates of the n-th target. Thus, the subspace processing cannot be applied in one step to the entire SAR scene. In this case, the SAR image has to be divided into subpatches over which the error function does not vary significantly; this implies that

$h_n(x,y)$ remains approximately the same in that subpatch (a condition which is met in practice). The signal subspace registration algorithm can then be applied to each subpatch.

Currently, along-track monopulse SAR data are being collected with DPCAs and the real data will be available soon. Reference [S98a] provides a study of the application of the signal subspace processing in MTD monopulse SAR for a simulated scenario. To test the proposed approach, we conducted a study using a realistic ISAR database which was collected by the radar group at the Navy's SPAWAR System, San Diego. The result of this study is described next.

3.5 Registration of ISAR Images

We have examined an X band ISAR database of an aircraft in [S99]. By separately processing the lower and upper portions of the slow-time domain ISAR data, we showed that the aircraft possessed some kind of rolling motion during the data acquisition. Figures 2a-b show the squint spatial domain ISAR reconstructions of this aircraft which are formed from the slow-time pulse numbers (PRIs) 89-152 and 105-168. These two overlapping 320-msec slow-time intervals (subapertures) are separated by 80 msec. (The PRF for this ISAR system is 200 Hz.)

These two images exhibit different point spread functions for each reflector on the aircraft; the variations of the PSF in the two images is also ***shift varying.*** These are due to two factors: the roll of the aircraft; and the dependence of the spotlight SAR PSF on the relative coordinates of a reflector with respect to the mid-point of the two subapertures (see Chapter 5). Thus, the ***magnitude*** of the two ISAR images of a reflector on the aircraft exhibit a relative shift as well as change in shape of PSF.

We wish to use the signal subspace processing to register the magnitudes of the two ISAR images in Figures 2a-b. For this we assign the reference image $f_1(x,y)$ and test image $f_2(x,y)$, respectively, to be the ISAR image in Figures 2a-b. As we stated earlier, the variations of the two ISAR images are shift-varying. Thus, we cannot apply the signal subspace processing, which assumes a common calibration error impulse function $h(x,y)$, throughout these two images.

However, we can assume that this impulse function is approximately shift-invariant within a relatively small area, or ***block***, in the reconstructed ISAR image. Clearly, we cannot choose an arbitrary small size block; the size of the block depends on the extent of a reflector PSF in the ISAR images. For this scenario, a block size of 7×15 in the spatial (x,y) domain is suitable.

Note that we also used the reconstructed ISAR images in the ***squint*** spatial domain. As we stated in Chapter 5, the spotlight SAR PSF of a reflector in the squint spatial domain appears to be a ***straight*** cross-shaped structure. For block-based processing, this

is more suitable than the *slanted* PSF in the original spatial domain.

The size of the filter also depends on the size of the pixels relative to the range and cross-range resolutions. For this example, the values of $(n_x, n_y) = (2, 4)$ are suitable; these correspond to a filter size of $(2n_x + 1, 2n_y + 1) = (5, 9)$.

Figure 2c is the difference image, $|f_2(x, y) - f_1(x, y)|$, for this example. This figure shows distinct vertical streaks which are due to the relative shift (mismatch) of the PSF of the reflectors which are caused by the roll of the aircraft. Figure 2d shows the subspace difference image, $|f_2(x, y) - \hat{f}_2(x, y)|$, in which most of those streaks have disappeared (that is, the ISAR image signatures are registered.) One can also see *patchy-looking* areas in the signal subspace difference image; this is caused by the block-based processing which introduces a different measure of similarity in each block; that is, some blocks are matched better than the others.

Finally, we did not use *complex* ISAR images in this example. The reason for this is that the overlapping slow-time data of the two sets of PRIs for this experiment (that is, pulse numbers 105-152) correspond to the same complex ISAR data and are perfectly calibrated. However, the coherent ISAR data in the non-overlapping PRIs (that is, pulse numbers 89-104 and 153-168) map into *disjoint* spectral (k_x, k_y) domain data for a given reflector (that is, they are orthogonal to each other). In this case, these complex data cannot be related by the model in Figure 1. The magnitude ISAR reconstructions provid two ISAR point spread functions which have slightly different coordinates and shapes that fit the system model in Figure 1.

4. Motion Tracking and Motion Flow Estimtaion in SAR/ISAR

One of the objectives of this investigation is to estimate the motion parameters of a moving target using a monopulse SAR system. A similar problem is also encountered in multistatic ISAR systems. The two SAR and ISAR problems are governed by a similar signal model. To test our proposed signal subspace motion tracking algorithm, we hav eutilized the X band ISAR data which we cited earlier. In the following, we outile the results of this study. First, we describe the signal model which is encounered in an ISAR system which utilizes a multistatic radar system.

4.1 Multistatic ISAR Model

The principles governing monopulse SAR may also be extended for the general problem of three-dimensional ISAR imaging and tracking with a single transmitter and multiple receivers; this is called a *multistatic* ISAR system. An example of a multistatic ISAR system is shown in Figure 3. Such an ISAR system can be used to retrieve three-dimensional information on spatial and motion parameters of an airborne aircraft. Some of the applications of this system include:

i. Automatic aircraft landing at the civilian and military airports;

ii. High-resolution three-dimensional air traffic control at the civilian airports;

iii. Studying vibration of various structures on an airborne aircraft which is useful for detecting structural flaws on an old aircraft, or designing safer aircrafts.

Linear (Constant Velocity) Motion Model: Suppose the transmitter of the multistatic ISAR system is located at the origin in the spatial (x, y, z) domain. Consider a moving reflector whose coordinates at the slow-time $\tau = 0$ is (x_n, y_n, z_n). When the target possesses a constant velocity, for example, (v_{xn}, v_{yn}, v_{zn}), its motion trajectory as a function of the slow-time is

$$\big(x_n - v_{xn}\,\tau, y_n - v_{yn}\,\tau, z_n - v_{zn}\,\tau\big).$$

The ISAR phase history of this target for a given receiver in the multistatic ISAR system of Figure 3 is dictated by its distance from the transmitting radar and that of the receiving radar. For example, for the ℓ-th receiver located at (x_ℓ, y_ℓ, z_ℓ), this round trip distance is

$$\sqrt{(x_n - v_{xn}\,\tau)^2 + (y_n - v_{yn}\,\tau)^2 + (z_n - v_{zn}\,\tau)^2} + \sqrt{(x_n - v_{xn}\,\tau - x_\ell)^2 + (y_n - v_{yn}\,\tau - y_\ell)^2 + (z_n - v_{zn}\,\tau - z_\ell)^2}.$$

It can be shown that, in theory, the user needs three receivers to determine the motion parameters of this reflector; for example, this can be achieved by the monostatic ISAR measurement and two bistatic ISAR measurements. The procedure for this involves first estimating the target speed

$$\sqrt{v_{xn}^2 + v_{yn}^2 + v_{zn}^2},$$

from the monostatic ISAR data [S99]. Then, this estimated speed is used to form the monostatic and bistatic ISAR images of the target. (The bistatic ISAR images are formed via first synthesizing monostatic ISAR data for an imaginary transmitting/receiving radar that is located at the midpoint of the line which connects the transmitting radar and the ℓ-th receiving radar.)

After digital spotlighting the n-th target image from its monostatic and bistatic ISAR reconstructions, the target phase history in the (ω, τ) domain can be formed for each image; these can be used to estimate the target parameters. One may also form various IF-ISAR image pairs from these reconstructions which can be translated into the target parameters (under the narrow-bandwidth and narrow-beamwidth assumption); this scheme, however, requires phase-unwrapping which is not feasible for an *isolated* reflector (not a contiguous region like a terrain).

In the case of resonating cavities and corner structures, the reflectors on the moving structure (aircraft) cannot be assumed to possess omni-directional amplitude patterns.

In this case, each reflector possesses a gain and phase history, which we identified as $a_n(\omega, x_n, y_n - u)$ in our work on SAR (see [S99, Chapter 3]), which varies with the radar frequency and aspect angle. This phase history corrupts the motion phase history of the reflector. However, provided that the receiving radars are relatively close to the transmitting radar, the target amplitude pattern is the same for the monostatic and bistatic ISAR measurements. Thus, the *relative phase difference* of the monostatic and bistatic ISAR images of the reflector still correspond to the reflector motion phase history. In other words, the target amplitude pattern phase history is transparent in *pair-wise* processing of multistatic ISAR images; the same is not true in processing the monostatic or a single bistatic ISAR image.

Nonlinear Motion and Maneuvering Target Model: In a realistic ISAR problem, a moving structure possesses nonlinear motion components in its flight path. Moreover, an airborne target, such as an aircraft, may contain maneuvers in its motion. In this case, the individual reflectors do not have *parallel* motion trajectories. For example, in the case of the ISAR data which were examined in Chapter 5, the reconstructions of the aircraft from its lower and upper ISAR data indicated a rotation in its motion.

In such scenarios, the motion trajectory of a reflector on the moving structure can be modeled via

$$\left[\, x_n - x_{en}(\tau)\ ,\ y_n - y_{en}(\tau)\ ,\ z_n - z_{en}(\tau)\,\right].$$

As we stated in Chapter 4, a practical approach to imaging such a structure is to treat the deviations from the *ideal* (linear) ISAR model as SAR motion errors. In this case, the user first estimates a constant speed for the entire structure, and forms its monostatic and bistatic ISAR images. Then, after digital spotlighting the prominent reflectors on the target, the monostatic and bistatic phase history of each prominent reflector can be formed and analyzed for motion estimation.

4.2 Motion Tracking via Signal Subspace Processing

In [S99], we showed that the signatures of a stationary reflector in the two slant plane monopulse SAR images appears shifted with respect to each other in the slant-range domain; the amount of shift is related to the relative height of the reflector in the slant plane. We used the signal subspace processing for estimating this shift in the slant-range domain.

A similar mathematical formulation can be used to show that, for the multistatic ISAR system of Figure 3, the signature of a reflector on the moving target in the ℓ-th bistatic ISAR image appears shifted with respect to its signature in the monostatic ISAR image; the shift is in both the slant-range and cross-range domains, and is related to the receiving

radar coordinates (x_ℓ, y_ℓ, z_ℓ) and the coordinates of the reflector at the slow-time zero, (x_n, y_n, z_n). By combining these shifts, the user could track the motion of each reflector on the moving structure (aircraft).

Next, we address the problem of estimating the relative shift in two images. Our approach is based on an application of the signal subspace processing of Section 3.1-3.3; a similar approach was used in estimating the relative slant-range shift in the two slant plane monopulse SAR images. For this, consider the system model in Figure 1. Suppose the impulse function in this model corresponds to a shift operation, for example,

$$h(x,y) = \delta\big(x - \Delta_{sx}, y - \Delta_{sy}\big),$$

where $(\Delta_{sx}, \Delta_{sy})$ are unknown, and the error function $f_e(x,y) = 0$; in this model, the variables (x,y) represent the slant-range and cross-range domains. In this case, the output of the two sensors are related via

$$f_2(x,y) = f_1\big(x - \Delta_{sx}, y - \Delta_{sy}\big).$$

Our objective is to estimate the shift pair $(\Delta_{sx}, \Delta_{sy})$.

Based on the solution in Section 3.3, we first identify the system in Figure 1 by the following discrete model:

$$f_2(x_i, y_j) = \sum_{m=-n_x}^{n_x} \sum_{n=-n_y}^{n_y} h_{mn}\, f_1(x_i - m\Delta_x, y_j - n\Delta_y),$$

where h_{mn}'s are the unknown coefficients which represent the samples of $h(x,y)$, and (Δ_x, Δ_y) are the pixel sample spacing in the (x,y) domain; that is, $\Delta_x = x_i - xi - 1$ and $\Delta_y = y_j - y_{j-1}$.

Let $\hat{h}_{mn}$'s be the estimate of h_{mn}'s for the above discrete model (see Section 3.3 for this solution). In this case, the relative shifts in the (x,y) domain can be determined from the moments of the estimated coefficients as shown in the following:

$$\hat{\Delta}_{sx} = \frac{1}{E_{\hat{h}}} \sum_{m=-n_x}^{n_x} \sum_{n=-n_y}^{n_y} m\Delta_x\, \hat{h}_{mn}^2$$

$$\hat{\Delta}_{sy} = \frac{1}{E_{\hat{h}}} \sum_{m=-n_x}^{n_x} \sum_{n=-n_y}^{n_y} n\Delta_y\, \hat{h}_{mn}^2,$$

with

$$E_{\hat{h}} = \sum_{m=-n_x}^{n_x} \sum_{n=-n_y}^{n_y} \hat{h}_{mn}^2,$$

where $(\hat{\Delta}_{sx}, \hat{\Delta}_{sy})$ are the estimated shifts in the (x, y) domain.

4.3 Motion Tracking in ISAR Images

As we mentioned earlier, monopulse SAR and ISAR systems have recently been built and their databases are becoming available for investigators. To show the application of the above-mentioned signal subspace processing for motion tracking, we consider the X band ISAR data of an airborne aircraft which was discussed earlier. This aircraft possesses a rolling motion; this can be demonstrated via the aircraft ISAR reconstructions from the lower synthetic aperture data $u \in [-L, 0]$, and the upper synthetic aperture data $u \in [0, L]$ [S99]. Those images indicated that the dominant reflectors on the wing of the aircraft exhibited an inward motion toward the fuselage.

We consider the two ISAR reconstructions of the aircraft which are formed via pulse numbers (PRIs) 81-144 and 89-152; the PRF for this ISAR system is 200 Hz. These two sets of PRIs correspond to two overlapping 320-msec synthetic aperture databases in the slow-time domain which are separated by 40 msec. We assign the two outputs of the sensors in Figure 1, $f_1(x, y)$ and $f_2(x, y)$, to be the ***magnitude*** of these two ISAR reconstructions in the squint spatial domain.

For signal subspace processing, we use a block size of 7×15 in the spatial (x, y) domain with $(n_x, n_y) = (2, 4)$ (that is, the filter size is $(2n_x+1, 2n_y+1) = (5, 9)$. Moreover, the algorithm is applied to a block-neighborhood around every pixel in the reconstructed image, a process which we refer to as ***overlapping block-based*** signal subspace processing.

The reason for using the ISAR reconstruction in the squint spatial domain is that the point spread function of a reflector in this domain appears to be a ***straight*** cross-shaped structure (see [S99, Chapter 5]). As a result, we can identify the region of support of a reflector in the ISAR image (that is, a block which is used for signal subspace processing) as a ***rectangle***.

We have emphasized throughout our work that the complex (coherent) SAR or ISAR images should be used for target detection, identification, multistatic tracking, etc. So, why did we use the magnitude of the ISAR image in this experiment? The overlapping slow-time data of the two sets of PRIs for this experiment (that is, pulse numbers 89-144) correspond to the same ISAR data; there is no relative shift which could be exploited for motion tracking in the same manner as in a multistatic ISAR system. The coherent data in the non-overlapping PRIs (that is, pulse numbers 81-88 and 145-152) yield the spatial frequency information on a given reflector in two ***disjoint*** spectral (k_x, k_y) bands (see [S99, Chapter 5]); thus, these cannot be related by the model in Figure 1.

In this case, the coherent signal subspace processing of the two ISAR images yields erroneous information. It is possible to perform SAR image compression on these two ISAR

images, and apply a spatial frequency domain lowpass (for example, a rectangular-shaped) filter to force the spectral signatures of a reflector in the two compressed ISAR images to possess a common spatial frequency band. Then, one can apply the signal subspace processing on the resultant complex images. This, however, brings up other issues which are beyond the scope of this report.

The magnitude ISAR images provides us with a simple and visible shift in the reconstructions which can be used to demonstrate the utility of the signal subspace processing in motion tracking. Figure 4 shows the resultant estimated motion flow for the dominant reflectors on the aircraft; the ISAR image of the aircraft is superimposed on this motion image. Note that the estimated motion vectors in Figure 4 indicate a slight inward movement of the dominant reflectors on the aircraft wings.

Next, we apply the overlapping block-based signal subspace processing to the two ISAR images which are formed from pulse numbers (PRIs) 89-152 and 105-168. These two overlapping 320-msec slow-time intervals are separated by 80 msec. Figure 5 shows the estimated motion vector for this scenario. Note that the inward motion of the dominant reflectors on the aircraft wings are more prominent in this image. Both Figures 4 and 5 exhibit some form of flow on the fuselage of the aircraft. The nature of these are not clear; some have suggested that these are patterns that are due to multiple scattering or surface waves.

References

[Har] M. Hartless and J. Barry, "Shipboard infrared search and track," Final Report of Contract N66001-94-C-6001, NCCOSC, December 1994.

[Leo] A. Leonov and K. Fomichev, *Monopulse Radar*, Translated by W. Barton, Artech House 1986.

[Sher] S. Sherman, *Monopulse Principles and Techniques,* Artech House, 1984.

[Sko] M.I. Skolnik, *Introduction to Radar Systems,* New York: McGraw Hill, 1980.

[S97a] M. Soumekh, "Moving target detection in foliage using along track monopulse synthetic aperture radar imaging," *IEEE Trans. Image Proc.*, vol. 6, no. 8, pp. 1148-1163, Aug. 1997.

[S98a] M. Soumekh, "Moving Target Detection and Automatic Target Recognition via Signal Subspace Fusion of Images," *Proceedings of SPIE's Annual International Symposium on Aerospace/Defense Sensing, Simulation, and Controls,* pp. 145-153, Orlando, April 1998.

[S99] M. Soumekh, *Synthetic Aperture Radar Signal Processing,* New York: Wiley, 1999 (in print).

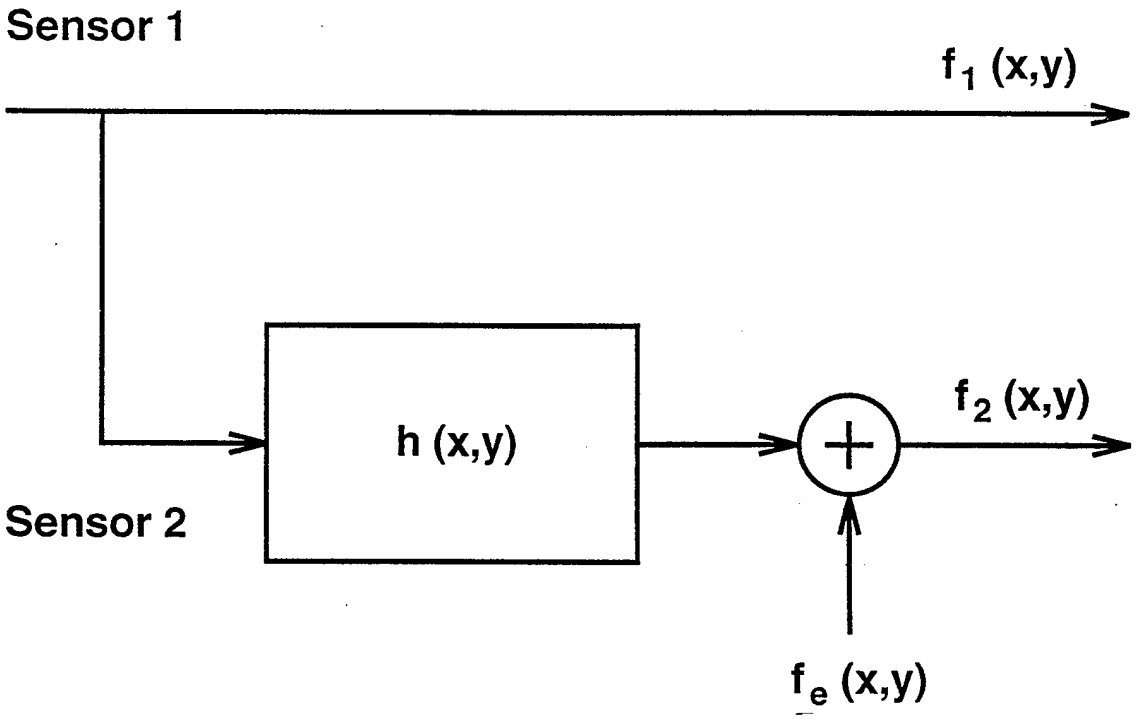

Figure 1

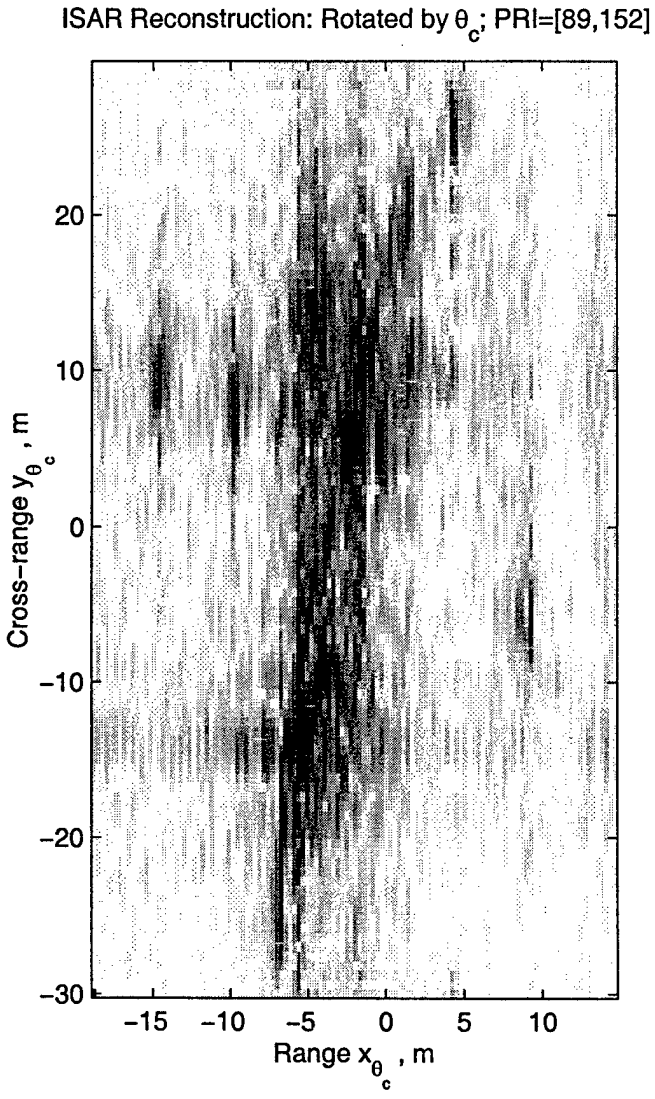
ISAR Reconstruction: Rotated by θ_c; PRI=[89,152]
20
10
0
−10
−20
−30
Cross−range y_{θ_c} , m
−15
−10
−5
0
5
10
Range x_{θ_c} , m

Figure 2a

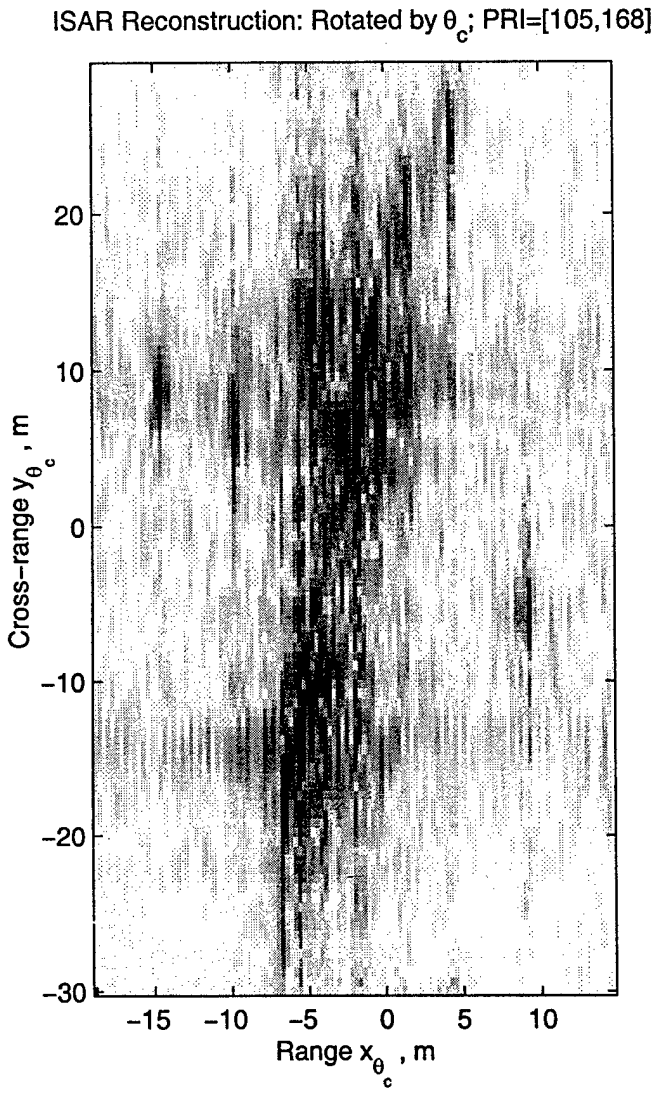
ISAR Reconstruction: Rotated by θ_c; PRI=[105,168]
20
10
0
−10
−20
−30
Cross−range y_{θ_c}, m
−15
−10
−5
0
5
10
Range x_{θ_c}, m

Figure 2b

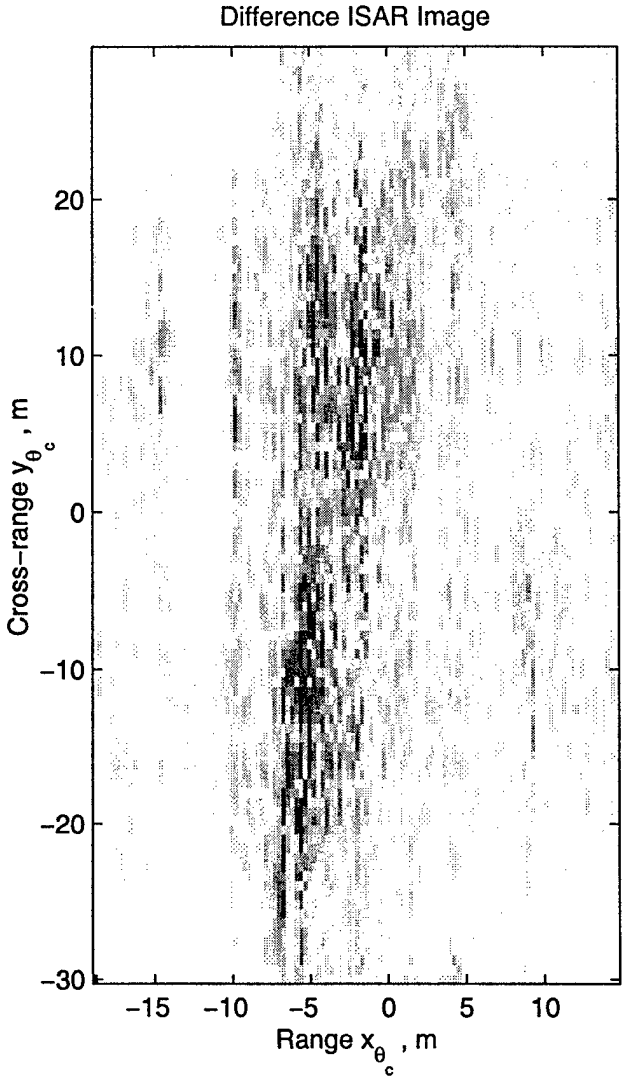
Difference ISAR Image
20
10
0
−10
−20
−30
Cross-range y_{θ_c} , m
−15
−10
−5
0
5
10
Range x_{θ_c} , m

Figure 2c

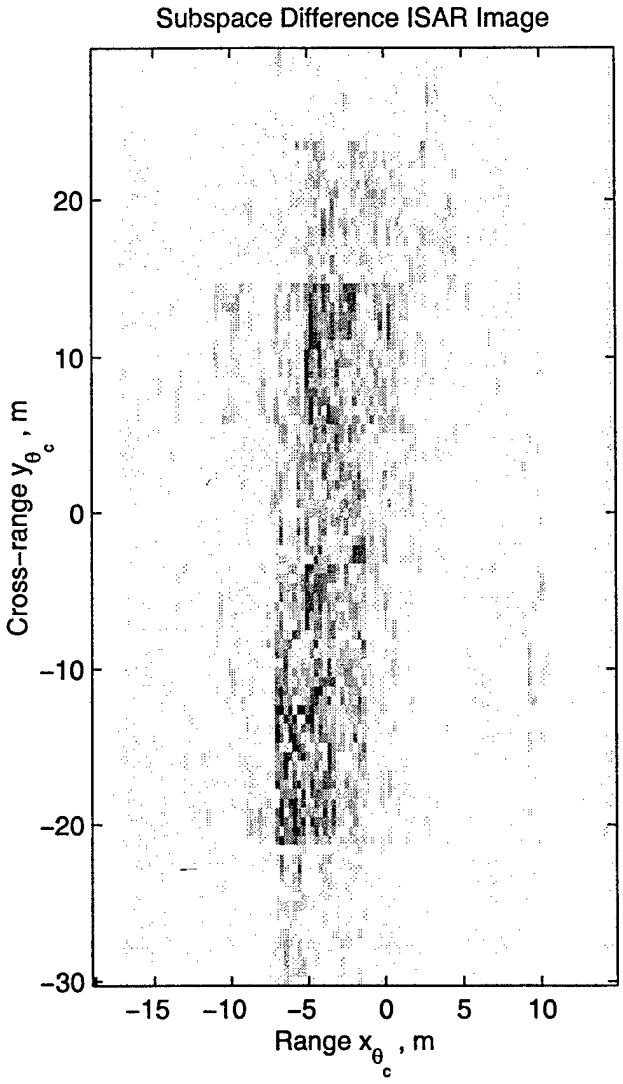
Subspace Difference ISAR Image
20
10
0
-10
-20
-30
Cross-range y_{θ_c} , m
-15
-10
-5
0
5
10
Range x_{θ_c} , m

Figure 2d

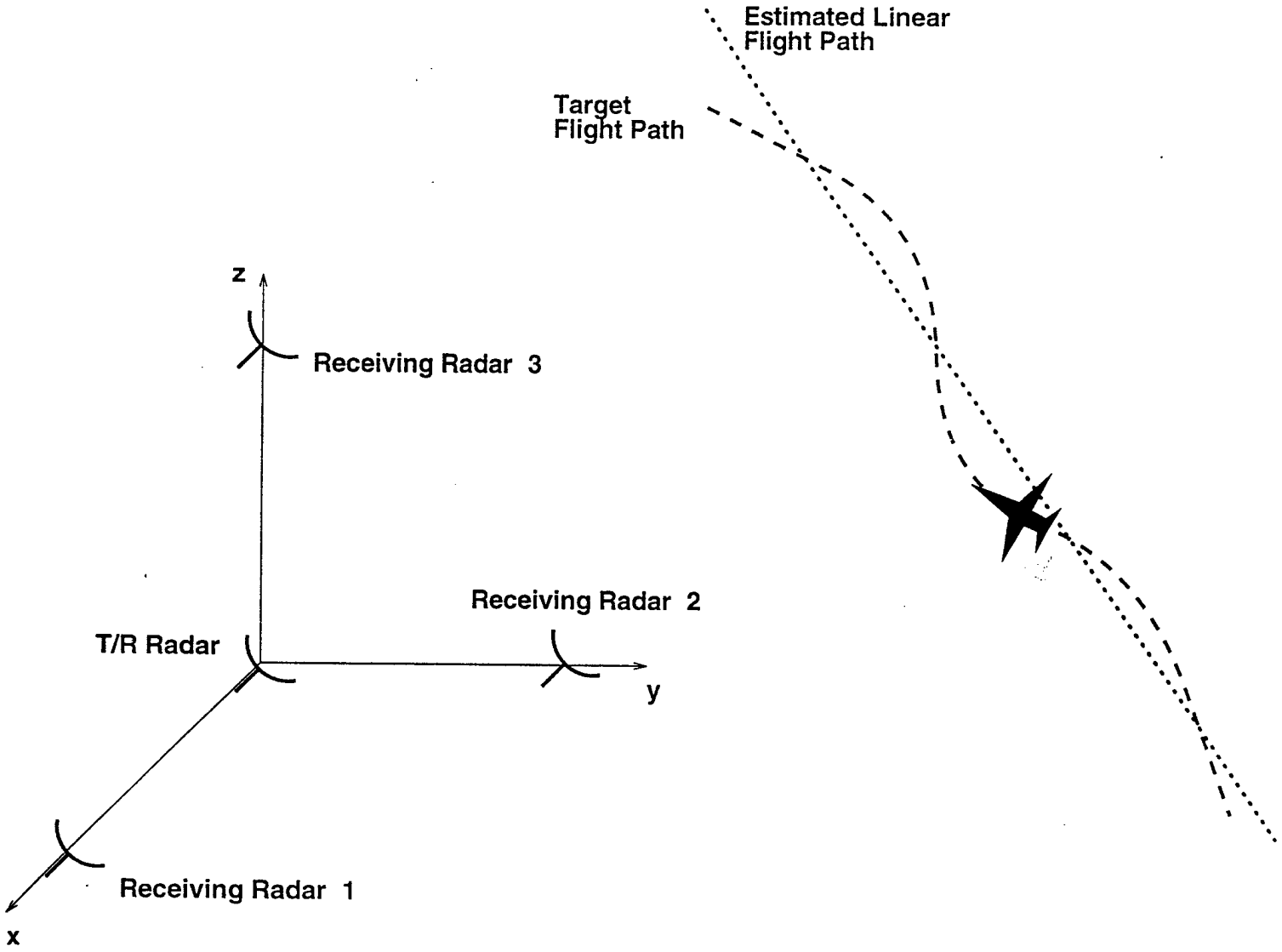
Estimated Linear
Flight Path
Target
Flight Path
z
Receiving Radar 3
Receiving Radar 2
T/R Radar
y
Receiving Radar 1
x

Figure 3

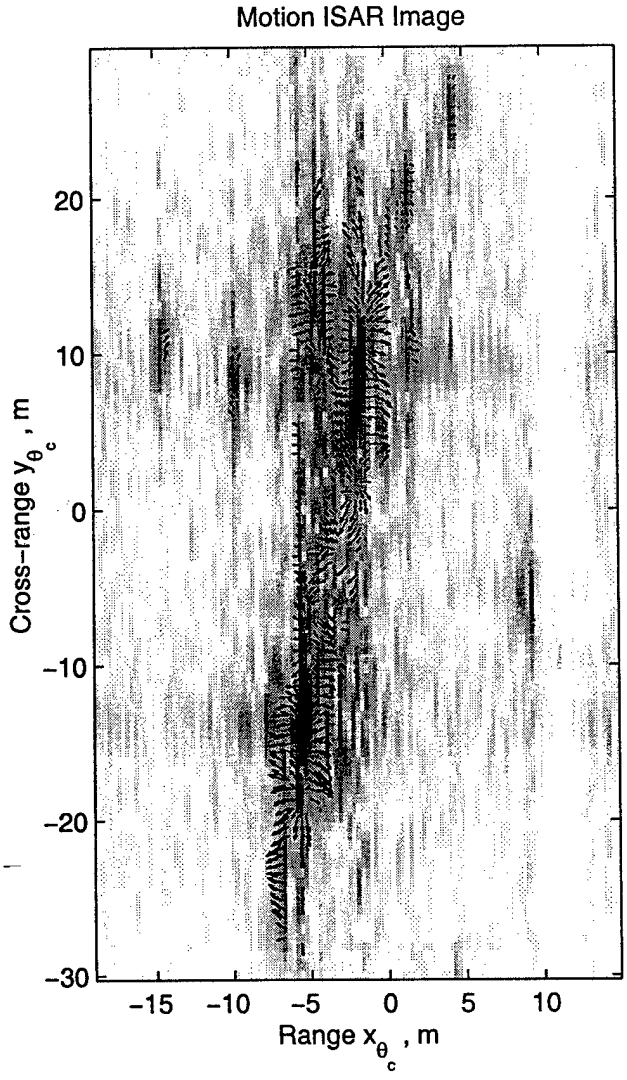
Motion ISAR Image
20
10
0
-10
-20
-30
Cross-range y_{θ_c} , m
-15
-10
-5
0
5
10
Range x_{θ_c} , m

Figure 4

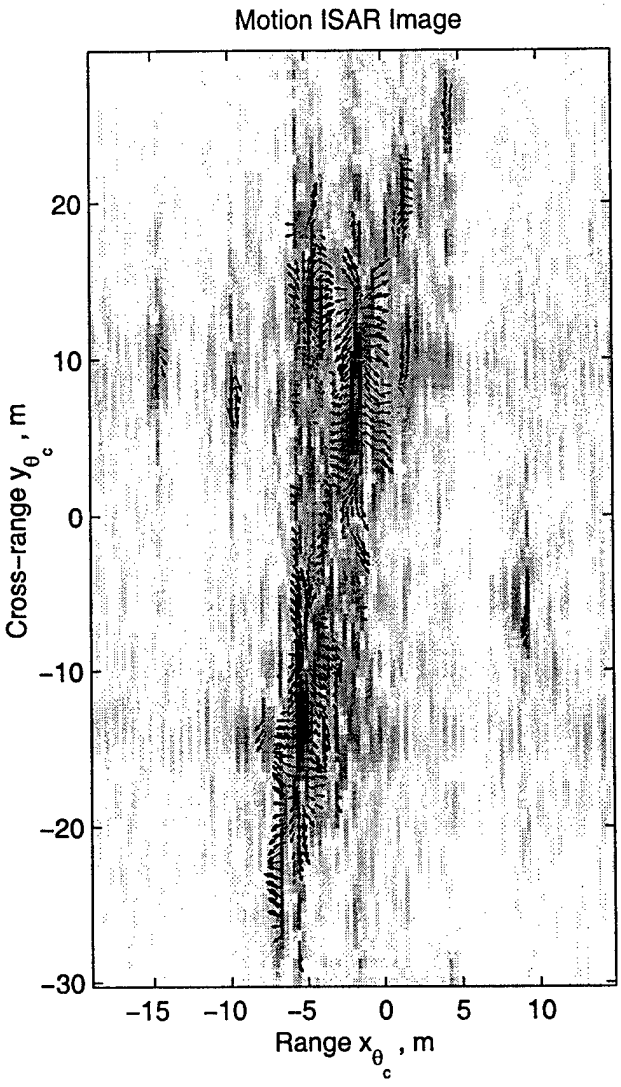
Motion ISAR Image
20
10
0
−10
−20
−30
−15
−10
−5
0
5
10
Cross−range y_{θ_c} , m
Range x_{θ_c} , m

Figure 5

REPORT DOCUMENTATION PAGE

Form Approved
OMB No. 0704-0188

1. AGENCY USE ONLY *(Leave blank)*	2. REPORT DATE	3. REPORT TYPE AND DATES COVERED
	10/21/98	Interim; 9/30/97-9/30/98

4. TITLE AND SUBTITLE
Moving Target Detection and Motion Estimation in Foliage Using Along Track Monopulse Synthetic Aperture Radar Imaging and Signal Subspace Processing of Uncalibrated MTD-SARs

5. FUNDING NUMBERS
N00014-96-0586 &
N00014-97-1-0966

6. AUTHOR(S)
Mehrdad Soumekh

7. PERFORMING ORGANIZATION NAMES(S) AND ADDRESS(ES)
Dept. of Electrical Engineering
201 Bell Hall
State University of New York at Buffalo
Buffalo, NY 14260

8. PERFORMING ORGANIZATION REPORT NUMBER

9. SPONSORING / MONITORING AGENCY NAMES(S) AND ADDRESS(ES)
Office of Naval Research
Ballston Centre Tower One
800 North Quincy Street
Arlington, VA 22217

10. SPONSORING / MONITORING AGENCY REPORT NUMBER

11. SUPPLEMENTARY NOTES

a. DISTRIBUTION / AVAILABILITY STATEMENT
Unlimited

12. DISTRIBUTION CODE

13. ABSTRACT *(Maximum 200 words)*

Our main goal at this stage of the investigation was to test the relative merits of the proposed signal subpace method with a realistic SAR/ISAR database. For this purpose, we utilized the ISAR data of an airborne commercial aircraft; the ISAR data were collected by the radar group at the Navy's SPAWAR System Center, San Diego. In the first stage of our study, we used the non-overlapping block-based implementation of the signal subspace algorithm for registering two ISAR images of the aircraft which were formed via two separate slow-time segments of the target flight path. We also used the overlapping block-based signal subspace processing to estimate the motion field of the ISAR images. The study with the realistic ISAR data revealed interesting properties of the ISAR signatures of the refelctors, cavities and surface structure for an airborne target.

14. SUBJECT TERMS	15. NUMBER OF PAGES
SAR, ISAR, FOPEN, MTD	24
	16. PRICE CODE

17. SECURITY CLASSIFICATION OF REPORT	18. SECURITY CLASSIFICATION OF THIS PAGE	19. SECURITY CLASSIFICATION OF ABSTRACT	20. LIMITATION OF ABSTRACT
Unclassified	Unclassified	Unclassified	